Model Predictions of Small-Angle Light Scattering from Films of Nematic Liquid Crystalline Polymers

F. Greco

Istituto G. Donegani, via Fauser 4-28100, Novara, Italy. *Received December 2, 1988; Revised Manuscript Received April 18, 1989*

ABSTRACT: A model is proposed to analyze scattering patterns in terms of randomly oriented dipoles of disclination lines of strength $|S| = {}^1/_2$. Comparison of the observed and calculated patterns is quite satisfactory: maxima in intensity are predicted in their correct positions, and their shift toward small θ-angle on annealing is generated by the increasing distance of the disclinations.

Introduction

The physical properties of nematic liquid crystalline polymers (LCP) are strongly dependent on the "degree of order" present in these materials. At a molecular level, it is possible to define an order parameter[1] which measures the distribution of the orientations of mesogenic units; at a supermolecular level, however, the concept of "degree of order" lacks of quantitative definition. As a matter of fact, macroscopic samples of LCP present no net order, because of the presence of various kinds of defects. These defects (disclinations) are discontinuities in the director field, directors being unit vectors indicating the average local orientation of mesogenic units.

Disclinations give rise to local excesses of free energy of the nematic liquid crystal; free energy relaxation leads to the reduction of their number density, possibly through annihilation of disclination pairs of opposite sign. A typical way to obtain the free energy relaxation is a heat treatment (isothermal annealing) on the mesophase state of the LCP. This process may be very important, since the disappearing of disclinations means an increasing size of the ordered regions of the material (sometimes this has been indicated as the "domain growth" process).

Thus, a better knowledge of the order in LCP, at a supermolecular level, can be gained if we have methods to control the spatial distribution of the disclinations and their dynamics; at present, two such methods are available: one is optical microscopy and the other is light scattering. This paper deals with the latter method.

Quite recently, some authors[2] have approached the problem of describing small-angle light-scattering (SALS) patterns for LCP: they developed a scattering theory for a model having isolated disclination lines contained in disks. The results indicated that the model is inadequate to describe the observed scattering. The authors also suggest that some combination of disclination multiplets might perhaps be adequate. So far, however, an "explanation" of the experimental data has not been worked out.

The purpose of this paper is to present a theoretical deduction of the observed SALS patterns, in the crossed polars (H_V) configuration. A brief review of experimental results (obtained by others) is presented in the first section, so as to show the "universality" of the problem (i.e., the common behaviour of all LCP). The other sections are dedicated to the exposition of a simple model, consisting in a collection of isolated disks, randomly oriented, each containing a disclination dipole together with the corresponding director field. The experimental patterns are compared with the theoretical patterns calculated by the model: the results of the comparison are fairly good, showing that this simple two-body interaction of the $S = \pm{}^1/_2$ disclinations can explain all the essential features of SALS experiments.

1. Review of Experimental Results

When all the directors lie in planes parallel to the glass plate on which a nematic LCP is placed, i.e., when we have a thin film of LCP, a typical Schlieren texture[3] can be observed under crossed polarizers. Disclinations are disposed on the dark lines ("dark brushes") of the texture and are oriented perpendicularly to the plane of the film.

The observation of the sample under crossed polars gives us the positions and the strength $|S|$ of the disclinations: in fact, a number of dark brushes which is equal to $4|S|$ emanates from each disclination line. The dark brushes indicate the regions where the optical axis of the material is parallel to one of the polars. To conclude, the sign of the strength of a disclination can be determined by observing the rotation of the dark brushes when the analyzer and polarizer are rotated together maintaining a crossed position: the sign is positive for the same direction of rotation and negative in the other case. Most of the experimental observations on thermotropic nematic LCP clearly show the predominance of lines of half-integer strength.[2,4]

Figure 1 is a schematic illustration of a typical H_V small-angle light-scattering pattern (the definitions of scattering and azimuthal angles (θ, μ) are given in Figure 2). The shape of the pattern is the same for all thermotropic LCPs investigated (see, for example, ref 5): patterns have a maximum scattered intensity at an angle $\theta = \theta_{max}$ and an azimuthal angle μ dependence with a fourfold symmetry. Maxima in intensity correspond to integer multiples of $\mu = {}^\pi/_2$; i.e., we have a four-leaf-clover pattern along the directions of the polarizer and analyzer (μ=0, ${}^\pi/_2$). "The unique patterns may reflect universal nature in the thermotropic nematic LCP" (quoted from ref 2).

Heat treatment (at a fixed temperature) generates a typical time evolution of Schlieren texture and corresponding H_V light-scattering patterns. A long annealing time coarsens the Schlieren texture, giving rise to an ordering process of the director field. Correspondingly, light-scattering patterns preserve their azimuthal dependence, but the maximum intensity increases and shifts to smaller θ-angles as the annealing time increases. These observations, too, are independent on the specific LCP, the only difference being the time scale of this kinetic behavior: stiff chains do present short relaxation times, while semiflexible LCPs change more slowly their textures and their LS patterns.[5]

In the next sections, a model capable of predicting these features of SALS patterns is presented. It will be shown that the shape of the patterns is generated by the dipolar

0024-9297/89/2222-4622$01.50/0

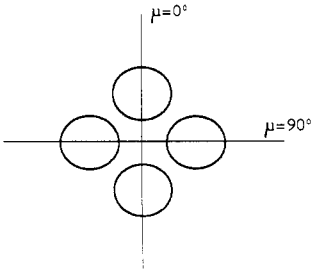

Figure 1. Sketch of a typical H_V scattering pattern from films of nematic liquid crystalline polymers.

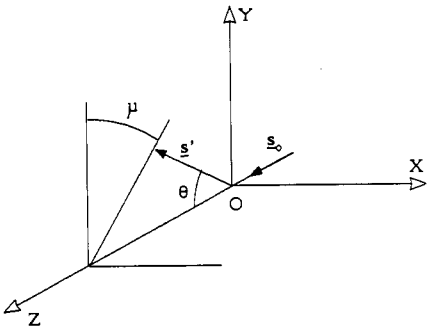

Figure 2. Cartesian coordinate system fixed to laboratory and definitions of various vectors and angles. $\mathbf{s}_0$ and $\mathbf{s}'$ are unit vectors along incident and scattered beams; θ and μ are the scattering and azimuthal angle, respectively.

interaction of disclinations, while the value of θ_{max} is linked to their average distance.

2. Coordinate Systems and Scattering Formulas

Figure 2 shows the coordinate system for the scattering experiments. $0XYZ$ is the Cartesian coordinate system fixed to the laboratory; $0Z$ is the propagation direction of the incident light beam (unit vector $\mathbf{s}_0$ coincides with unit vector $\mathbf{Z}$), while the propagation direction of the scattered ray is specified by the unit vector $\mathbf{s}'$. The scattering pattern is recorded by a two-dimensional detector (usually a photographic plate or an array of photodiodes) placed normal to $0Z$. A point of the pattern is specified by the scattering angle θ and the azimuthal angle μ.

The material is placed on the $0XY$ plane, and the scattering is investigated for the normal incidence configuration. As we consider H_V polarization conditions, polarizer and analyzer are disposed along the vertical direction $0Y$ and the horizontal direction $0X$, respectively. Let us consider a planar disclination dipole; the Cartesian coordinate system $0xyz$ fixed to the dipole is shown in Figure 3. The axis $0z$ coincides with $0Z$ and is parallel to the disclination lines; the plane of the dipole $0xy$ lies in the plane $0XY$. The $0x$-axis makes an angle Ω with respect to the $0X$-axis fixed to the laboratory. So, systems $0XYZ$ and $0xyz$ differ only by a rotation around the $0Z$-axis, the transformation equations between unit vectors being

$$\mathbf{X} = \cos\Omega\,\mathbf{x} - \sin\Omega\,\mathbf{y}$$
$$\mathbf{Y} = \sin\Omega\,\mathbf{x} + \cos\Omega\,\mathbf{y} \qquad (2.1)$$

In the context of the Rayleigh–Born approximation (see ref 6), which will be used in this paper, the total scattered amplitude under H_V polarization conditions is given by

$$E = c\int\int\int_v \mathbf{M}(\mathbf{r})\cdot\mathbf{A}\,\exp(i\mathbf{k}\cdot\mathbf{r})\,dV \qquad (2.2)$$

where c is a constant depending on the geometry of the scattering apparatus, $\mathbf{A}$ is the unit vector of the analyzer

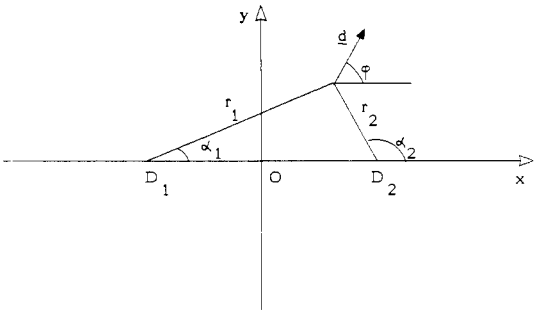

Figure 3. Cartesian coordinate system fixed to a disclination dipole (disclinations are located at points D_1, D_2). $0x$-axis makes an angle Ω with respect to the $0X$-axis fixed to the laboratory. (r_1, r_2) and (α_1, α_2) are needed in defining bipolar coordinates (see section 4). $\mathbf{d}$ is the director.

(in our case $\mathbf{A} = \mathbf{X}$), and $\mathbf{k}$ is the scattering vector defined by

$$\mathbf{k} = \mathbf{k}(\theta,\mu) = (2\pi/\lambda)(\mathbf{s}_0 - \mathbf{s}') \qquad (2.3)$$

λ is the wavelength within the medium, and $\mathbf{M}(\mathbf{r})$ is the polarization induced in the volume element located at point $\mathbf{r}$ (see section 3). When the volume V containing the material reduces to a surface Σ, we have simply to substitute eq 2.2 with the following:

$$E = c\int\int_\Sigma \mathbf{M}(\mathbf{r})\cdot\mathbf{A}\,\exp(i\mathbf{k}\cdot\mathbf{r})\,d\sigma \qquad (2.4)$$

Since surface Σ lies on the plane $0XY$, in expressing the scalar product $\mathbf{k}\cdot\mathbf{r}$ we only need the projection of $\mathbf{k}$ on $0XY$, i.e., the projection of $\mathbf{s}'$ on $0XY$. Let us term $\mathbf{s}'_P$ this projection and $\mathbf{s}'_{PX}$ and $\mathbf{s}'_{PY}$ its components along X and Y. From Figure 2 we have

$$|\mathbf{s}'_P| = \sin\theta$$
$$\mathbf{s}'_{PX} = \sin\theta\sin\mu\,\mathbf{X}$$
$$\mathbf{s}'_{PY} = \sin\theta\cos\mu\,\mathbf{Y} \qquad (2.5)$$

It is convenient to express the scalar product $\mathbf{k}\cdot\mathbf{r}$ in the Cartesian coordinate system $0xyz$. By using eq 2.1, we can rewrite eq 2.5

$$\mathbf{s}'_{PX} = \sin\theta\sin\mu(\cos\Omega\,\mathbf{x} - \sin\Omega\,\mathbf{y})$$
$$\mathbf{s}'_{PY} = \sin\theta\cos\mu(\sin\Omega\,\mathbf{x} + \cos\Omega\,\mathbf{y})$$

or, by calling $\mathbf{s}'_{P_x}$ and $\mathbf{s}'_{P_y}$ the components of $\mathbf{s}'_P$ along $\mathbf{x}$ and $\mathbf{y}$

$$\mathbf{s}'_{P_x} = \sin\theta(\sin\mu\cos\Omega + \cos\mu\sin\Omega)\mathbf{x} = \sin\theta\sin(\mu+\Omega)\mathbf{x}$$
$$\mathbf{s}'_{P_y} = \sin\theta(\cos\mu\cos\Omega - \sin\mu\sin\Omega)\mathbf{y} = \sin\theta\cos(\mu+\Omega)\mathbf{y} \qquad (2.6)$$

Then we can write

$$\mathbf{k}\cdot\mathbf{r} = -(2\pi/\lambda)\sin\theta[x\sin(\mu+\Omega) + y\cos(\mu+\Omega)] \qquad (2.7)$$

3. Anisotropy and Director Field of a Dipole

Let us suppose that the polarization vector $\mathbf{M}(\mathbf{r})$ is linearly related to the electric field $\mathbf{E}(\mathbf{r})$. In general, the field $\mathbf{E}(\mathbf{r})$ differs from the external field of the incident light because of the presence of the surrounding material; the Rayleigh–Born approximation neglects these perturbing effects of the "internal" field. Under vertical polarization conditions, we therefore write

$$\mathbf{E}(\mathbf{r}) = E_0\mathbf{Y}$$

In our case, the medium polarizes anisotropically, so we should use the polarizability tensor α. However, it can be shown[7] that, if we impose uniaxiality of the material, the resulting expression for $\mathbf{M}(\mathbf{r})$ is

$$\mathbf{M}(\mathbf{r}) = E_0[\delta(\mathbf{d}(\mathbf{r})\cdot\mathbf{Y})\mathbf{d}(\mathbf{r}) + \alpha\mathbf{Y}] \tag{3.1}$$

where $\mathbf{d}(\mathbf{r})$ is a unit vector in the direction of the (local) optical axis, α is the polarizability perpendicular to the optical axis, and δ is the optical anisotropy, i.e., the difference of polarizabilities parallel and perpendicular to the optical axis.

It is now possible to calculate the scalar product $\mathbf{M}\cdot\mathbf{A}$. The term $\alpha E_0\mathbf{Y}$ in eq 3.1 gives zero when multiplied by $\mathbf{A}$ (because $\mathbf{A} = \mathbf{X}$). So we have

$$\mathbf{M}\cdot\mathbf{A} = E_0\delta(\mathbf{d}\cdot\mathbf{X})(\mathbf{d}\cdot\mathbf{Y})$$

In the coordinate system $0xy$, unit vector $\mathbf{d}$ is identified by the angle ϕ with respect to the x-axis (Figure 3). Then

$$\mathbf{d}\cdot\mathbf{X} = \cos(\phi+\Omega)$$

$$\mathbf{d}\cdot\mathbf{Y} = \sin(\phi+\Omega)$$

and

$$\mathbf{M}\cdot\mathbf{A} = (E_0\delta/2)\sin[2(\phi+\Omega)] \tag{3.2}$$

It is important to note in eq 3.1 that if one makes the substitution $\mathbf{d}' = -\mathbf{d}$, i.e., if one considers the angle $\phi' = \pi + \phi$ in eq 3.2, the calculated value of $\mathbf{M}\cdot\mathbf{A}$ remains unchanged. This means that the scalar product $\mathbf{M}\cdot\mathbf{A}$ depends on the orientation identified by the unit vector $\mathbf{d}$ but not on its direction: it must be so, of course, because if the molecules are nonpolar or, if polar, are distributed with equal likelihood in both directions corresponding to a given orientation, the sign of $\mathbf{d}$ is arbitrary.

Equations 3.1 and 3.2 are valid for any optically anisotropic uniaxial medium. To introduce the additional information that the medium is a liquid crystal, we have to *identify the orientation of the optical axis with the director* describing the local average molecular orientation. In this way, we can use the results of the continuum mechanical theory for nematics[8] to give the field $\phi(P)$ to insert in eq 3.2. In his classical paper,[9] Frank gives the equilibrium equation for a planar director field and the specific solution for the case of a single discontinuity. His treatment is based on the "one-constant approximation"; i.e., the relevant elastic constants (bend and splay) are taken to be equal. This approach can be generalized[1] to our case, in which there are two discontinuities of opposite strength separated by a distance L (a disclination dipole); the solution is

$$\phi = |S|(\alpha_1 - \alpha_2) + \phi_0 \tag{3.3}$$

α_1 and α_2 being the polar angles relative to each line (see Figure 3). Angle ϕ_0 is determined by the boundary conditions; this is a point which deserves further comment (see section 5).

The next step now should be to express the polar angles α_1 and α_2 in terms of coordinates x and y; however, this leads to a very complicated form for the integral eq 2.4. On the contrary, a suitable choice of a different coordinate system can greatly simplify the resulting expressions: this will be considered in the next section.

4. Bipolar Coordinate System and the Domain of Integration

The form of expression 3.3 suggests the following choice for the "natural" coordinate system of the problem:

$$u = \alpha_1 - \alpha_2$$

$$v = \ln(r_1/r_2) \tag{4.1}$$

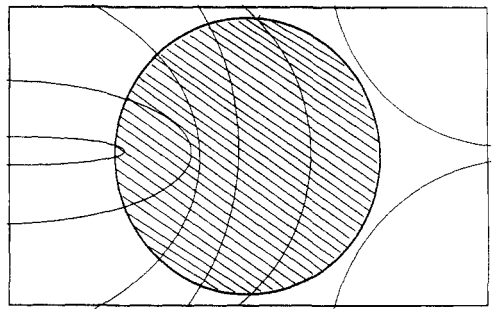

Figure 4. Sketch of the director field of a dipole; the dashed disk is the integration domain chosen to calculate scattered intensity.

Coordinates (u, v) defined by (4.1) are called bipolar coordinates (Figure 3). The transformation equations are

$$x = (L/2)\frac{\sinh v}{\cosh v - \cos u}$$

$$y = (L/2)\frac{-\sin u}{\cosh v - \cos u} \tag{4.2}$$

The Jacobian of the transformation is

$$J = \frac{-(L/2)^2}{(\cosh v - \cos u)^2} \tag{4.3}$$

By inserting eq 4.1 and 4.2 in eq 2.7, 3.2, and 3.3, we have

$$f(u,v) \equiv \mathbf{k}\cdot\mathbf{r} = -(L/\lambda)\pi\sin\theta\left[\sin(\mu+\Omega)\frac{\sinh v}{\cosh v - \cos u} - \cos(\mu+\Omega)\frac{\sin u}{\cosh v - \cos u}\right] \tag{4.4}$$

$$\phi = |S|u + \phi_0 \tag{4.5}$$

$$\mathbf{M}\cdot\mathbf{A} = (E_0\delta/2)\sin[2(|S|u + \phi_0 + \Omega)] \tag{4.6}$$

The integration domain of the integral (2.4) still has to be established. The only physically measurable characteristic dimension of the problem is length L (distance of two disclination); thus, the area of domain Σ must certainly be of order L^2. In order to simplify the calculations, the simplest possible shape for Σ will be adopted, i.e., an isolated disk with diameter L containing a disclination dipole on its perimeter and the director field $\mathbf{d}$ (given by eq 4.5) as its internal structure (Figure 4). It has to be stressed that the circle $\partial\Sigma$ is a coordinate curve in our variables (u, v), and this considerably simplifies the integration. With reference to Figures 3 and 4, since in the upper part ($y > 0$) of the circle it is

$$0 < \alpha_1 < \pi/2 \quad \text{and} \quad \pi/2 < \alpha_2 < \pi$$

the geometric relation

$$\alpha_1 + (\pi - \alpha_2) = \pi/2$$

becomes

$$u = -\pi/2$$

Similarly, since in the lower part ($y < 0$) of the circle it is

$$3\pi/2 < \alpha_1 < 2\pi \quad \text{and} \quad \pi < \alpha_2 < 3\pi/2$$

the geometric relation

$$(2\pi - \alpha_1) + (\alpha_2 - \pi) = \pi/2$$

becomes

$$u = \pi/2$$

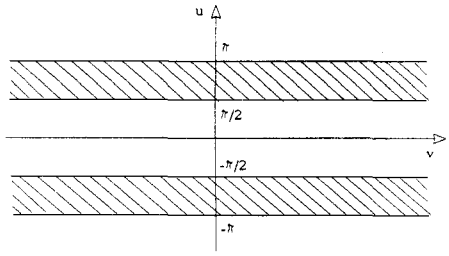

Figure 5. Integration domain for integral (4.7) in the (u, v) plane of bipolar coordinates.

That portion of the x-axis included between the disclinations can be described by

$$\alpha_1 = 0 \quad \text{and} \quad \alpha_2 = \pi; \quad u = -\pi \quad \text{(case A)}$$

$$\alpha_1 = 2\pi \quad \text{and} \quad \alpha_2 = \pi; \quad u = \pi \quad \text{(case B)}$$

Cases A or B correspond respectively to the two possibilities

$$y \to 0^+ \quad \text{(A)}$$
$$y \to 0^- \quad \text{(B)}$$

The two disclinations are identified by $v = \pm\infty$. Then the integration domain Σ will be the union of two infinite strips (Figure 5). Σ is identified by

$$u \in [-\pi, -\pi/2] \cup [\pi/2, \pi]$$
$$v \in [-\infty, \infty]$$

Using eq 4.4, 4.6, and 4.3 and imposing $|S| = {}^1/_2$, we obtain the following explicit form for the integral (2.4):

$$E = (cE_0\delta/8)L^2 \int\int_\Sigma \sin\,[u+2(\phi_0+\Omega)] \exp\left(i \left[\sin\,(\mu+\Omega)\,\frac{\sinh v}{\cosh v - \cos u} - \cos\,(\mu+\Omega)\,\frac{\sin u}{\cosh v - \cos u} \right] [-(L/\lambda)\pi \sin\theta] \right) \frac{du\,dv}{(\cosh v - \cos u)^2} \quad (4.7)$$

We can see from eq 4.7 that the integrand function diverges if and only if the Jacobian (4.3) diverges, i.e., if and only if it results

$$v = 0 \qquad u = 0 \quad (4.8)$$

However, eq 4.8 cannot hold simultaneously in our integration domain ($u = 0$ describes those portions of the x-axis external to the disclinations); thus the integrand function can never diverge.

5. Formulas for the Scattered Intensity

Equation 4.7 is the essential result of the model. It is convenient, however, to manipulate it in order to obtain something easier to handle. Straightforward calculations show that eq 4.7 is completely equivalent to

$$E = (cE_0\delta/2)L^2 \left(\sin\,[2(\phi_0+\Omega)] \int_{\pi/2}^{\pi} du \int_0^{\infty} dv\, I^2(u,v) \cos u \cos f + i \cos\,[2(\phi_0+\Omega)] \int_{\pi/2}^{\pi} du \int_0^{\infty} dv\, I^2(u,v) \sin u \sin f \right) \quad (5.1)$$

where function $I(u,v)$ is defined by

$$I(u,v) = (\cosh v - \cos u)^{-1} \quad (5.2)$$

and the function $f(u,v)$ was defined by eq 4.4.

Using the addition formula for $\sin\,[2(\phi_0+\Omega)]$ and $\cos\,[2(\phi_0+\Omega)]$, we can rewrite eq 5.1:

$$E = (cE_0\delta/2)L^2[(\sin 2\phi_0 \cos 2\Omega + \cos 2\phi_0 \sin 2\Omega) I_{CC} + i(\cos 2\phi_0 \cos 2\Omega - \sin 2\phi_0 \sin 2\Omega) I_{SS}] \quad (5.3)$$

where functions I_{SS} and I_{CC} are defined by

$$I_{CC} = \int_{\pi/2}^{\pi} du \int_0^{\infty} dv\, I^2(u,v) \cos u \cos f$$
$$I_{SS} = \int_{\pi/2}^{\pi} du \int_0^{\infty} dv\, I^2(u,v) \sin u \sin f \quad (5.4)$$

The intensity of scattering is proportional to the square modulus of the amplitude:

$$\mathcal{I} = K|E|^2 = K(cE_0\delta/2)^2L^4[I_{CC}^2(\sin^2 2\phi_0 \cos^2 2\Omega + \cos^2 2\phi_0 \sin^2 2\Omega + 2 \sin 2\phi_0 \cos 2\phi_0 \sin 2\Omega \cos 2\Omega) + I_{SS}^2(\cos^2 2\phi_0 \cos^2 2\Omega + \sin^2 2\phi_0 \sin^2 2\Omega - 2 \sin 2\phi_0 \cos 2\phi_0 \sin 2\Omega \cos 2\Omega)] \quad (5.5)$$

Equation 5.5 gives the intensity of scattered light for a disclination dipole whose x-axis makes an angle Ω with the X-axis of the analyzer.

Up to now, angle ϕ_0 (see eq 3.3 and 4.5) has been left arbitrary. I will make here the *hypothesis* that only the two "special" values $\phi_0 = 0$ and/or $\phi_0 = \pi/2$ are allowed; this corresponds to a director field at infinity parallel ($\phi_0 = 0$) or perpendicular ($\phi_0 = \pi/2$) to the dipole axis. At present, there appears to be no way of physically justifying this choice: it might be linked to the relative energetical stability of the configurations corresponding to different ϕ_0.[10] The energies of these different configurations could also be different, if we make the computations without resorting to the "one-constant approximation" (see section 3). As a matter of fact, however, all experimental observations of isolated disclination dipoles show that $\phi_0 = 0$.[11,12]

With this hypothesis on ϕ_0, eq 5.5 becomes

$$\mathcal{I} = K(cE_0\delta/2)^2L^4[(\sin^2 2\Omega)I_{CC}^2 + (\cos^2 2\Omega)I_{SS}^2] \quad (5.6)$$

which is obtained for $\phi_0 = 0$ as well as for $\phi_0 = \pi/2$. To obtain the total scattered intensity from an assembly of randomly oriented dipoles, one merely sums the individual scattered intensities. This procedure presumes that dipoles scatter incoherently. Averaging over Ω gives

$$\mathcal{I} = NK(cE_0\delta/2)^2L^4/(2\pi) \int_0^{2\pi} d\Omega\, [(\sin^2 2\Omega)I_{CC}^2 + (\cos^2 2\Omega)I_{SS}^2] \quad (5.7)$$

where N is the total number of dipoles.

6. Results of Numerical Integration

Listed below are the relevant formulas obtained in the previous sections (front factors are omitted):

$$\mathcal{I} = \int_0^{2\pi} d\Omega\, [(\sin^2 2\Omega)I_{CC}^2 + (\cos^2 2\Omega)I_{SS}^2] \quad (6.1)$$

$$I_{CC} = \int_{\pi/2}^{\pi} du \int_0^{\infty} dv\, I^2(u,v) \cos u \cos f$$

$$I_{SS} = \int_{\pi/2}^{\pi} du \int_0^{\infty} dv\, I^2(u,v) \sin u \sin f \quad (6.2)$$

$$f(u,v) = -(L/\lambda)\pi \sin\theta\, I(u,v)^* [\sin\,(\mu+\Omega) \sinh v - \cos\,(\mu+\Omega) \sin u] \quad (6.3)$$

$$I(u,v) = (\cosh v - \cos u)^{-1} \quad (6.4)$$

These equations were programmed in Fortran for a UNISYS 1100/80 (computer programs are available from

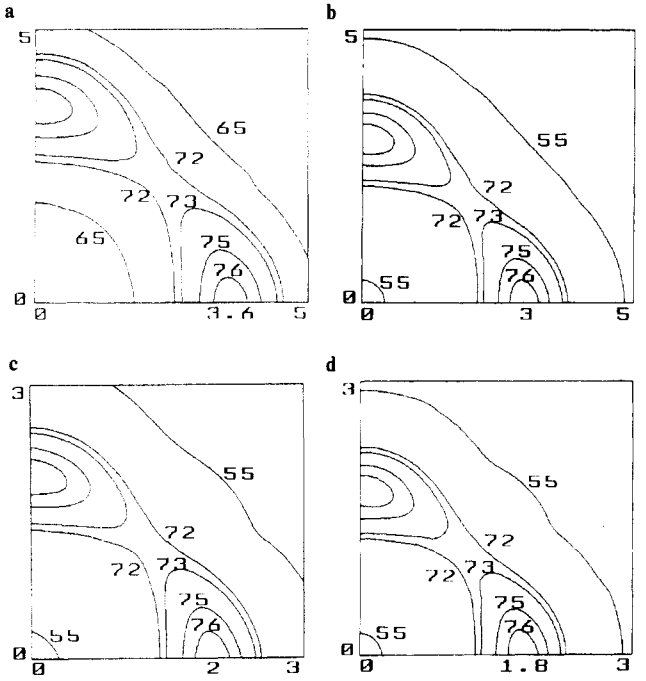

Figure 6. Calculated H_V scattering contours for L = 5, 6, 9, and 10 μm (parts a, b, c, and d, respectively); only a portion of each pattern is shown (i.e., the first quadrant: $0° \leq \mu \leq 90°$). The value of θ_{max} decreases as L increases. Note the different scales in parts a and b versus parts c and d.

Dr. L. Caccianotti and/or the present author at Donegani). The resulting values for the scattered intensity were subsequently inserted into an interpolation procedure in order to produce the isointensity contour plots in the θ,μ plane. These plots are the computed simulations of the experimental scattering patterns; to simulate the observed change of the patterns with annealing, the calculation procedure has been repeated for several different values of L.

Figure 6 shows computed H_V scattering contours for four different values of L. All scattering contours are calculated by eq 6.1, i.e., without the front factor $NK(cE_0\delta/2)^2L^4/2\pi$ (see eq 5.7). Inspection of these patterns shows immediately that, in spite of the simplicity of the assumptions, the predictions of the model are extremely good: the scattering maxima are indeed located at $\mu = 0$ and $\mu = \pi/2$; the value of θ_{max} decreases as length L increases. A more extensive collection of scattering patterns than reported in Figure 6 has been worked out. They further confirm these predictions.

A detailed inspection of tabulated data (not reported here) shows that patterns are not perfectly symmetric with respect to the axis $\mu = \pi/4$: intensities are a bit larger at azimuthal angle μ than they are at $(\pi/2) - \mu$. This difference grows as θ increases. However, differences are so small (less than 2%) that they could also be a spurious effect of numerical computations. To test this point, computations have been repeated in double precision, but results did not change. It should be mentioned, however, that the integration routine (IMSL library, routine DMLIN) was not directly accessible, and therefore its precision is not under direct control. In any event, also if this slight asymmetry were intrinsic to the phenomena, it might prove difficult to be experimentally detected. One possible source of asymmetry is the fact that the analyzer is not strictly perpendicular to the scattered beam, the more so the larger θ.

Figure 7 shows a plot of the angle θ_{max} as a function of the reduced variable L/λ. On the basis of their experimental data, Hashimoto et al.[2] have suggested that θ_{max} could be proportional to $1/L$. According to this suggestion, the analytic expression $\theta_{max} = a/(L/\lambda)$ has been fitted to our calculated values of θ_{max} corresponding to different ratios L/λ; the fit was excellent with a = 36.4, showing that Figure 7 is in fact the plot of an hyperbola.

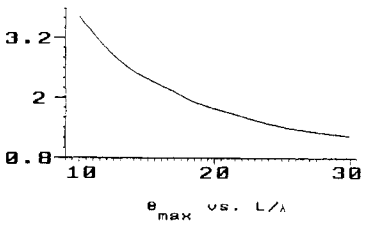

Figure 7. Plot of the law $\theta_{max} = \theta(L/\lambda)$, which is predicted by the model; it has been assumed λ = 0.5 μm.

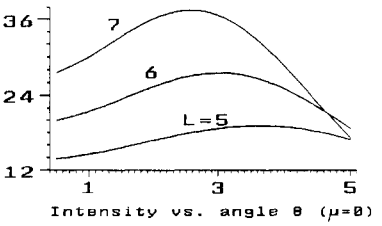

Figure 8. H_V intensity distribution (at 0° azimuthal angle) calculated for various values of L. Maximum intensity increases as L increases.

The "universal" (i.e., independent of the specific material) curve of Figure 7 gives us the possibility of making a quick evaluation of the average spacing between disclination from light-scattering data. So, time-resolved small-angle light scattering, when used in connection with the present results, gives the kinetic behavior of the defect lines, i.e., the law $L = L(t)$ which describes their (average) relative motion.

In Figure 8, the scattered light intensity is plotted against θ (at 0° azimuthal μ angle) for various values of L. To compare intensities corresponding to different L, we should remember that the area of the film which is observed remains constant during annealing. Therefore, N in eq 5.7 must be taken inversely proportional to L^2. By further considering that in the front factor of eq 5.7 the product NL^4 appears, we take the results of eq 6.1 multiplied by L^2. Figure 8 quantitatively shows the increase of maximum intensity as well as the previously mentioned shift to smaller θ angles as L increases. Figure 8 should be compared with Figure 2 in ref 13. The comparison shows a very good qualitative agreement. For a quantitative prediction of intensity, we would need the measured value of optical anisotropy δ, but these data are unavailable to the present writer.

Before concluding, one might ask whether the use of a disk as an integration domain for the integral (2.4) strongly affects the results, i.e., whether the results themselves are a lucky consequence of a purely arbitrary choice. To answer this question, computations have been repeated by changing the boundary of region Σ. For the sake of simplicity, however, the condition that $\partial\Sigma$ is a coordinate curve in the variables u and v has been preserved (see section 4). Since coordinate curves in the bipolar system are circumferences, the integration domain is now the union of four circles, taking the shape of a "four-leaf clover". (Obviously, this shape of the integration domain should not be confused with the somewhat analogous shape of the scattering pattern. In fact, the latter is already obtained by integration on a disk.)

These tests showed that the results are fundamentally "stable"; i.e., the shape of the patterns turns out to be essentially the same as for the disk case. This confirms that the key point in the model is *the choice of the dipolar interaction.*

7. Conclusions

It has been shown that a simple model of two-body interactions between disclinations can account well for the experimental scattering patterns from LCP films. The presence of scattering maxima in the patterns can be predicted without using the concept of interference, which would be difficult to associate to a random orientation of the dipoles. The only parameter of the model (length L) is sufficient to explain the time evolution of the patterns. Further work on the V_V pattern is in progress.

Acknowledgment. I am most grateful to Professor G. Marrucci (University of Naples) for always being willing to let me have the benefit of his opinions. My thanks go to Dr. L. Abbondanza and Dr. L. Caccianotti, my friends and colleagues at Donegani, for many stimulating discussions and personal cooperation. Specifically, I wish to express my warmest thanks to Dr. L. Caccianotti for putting his computing experience at my disposal.

References and Notes

(1) de Gennes, P.-G. *The physics of liquid crystals*; Clarendon Press: Oxford, 1974.
(2) Hashimoto, T.; Nakai, A.; Shiwaku, T.; Hasegawa, H.; Rojstaczer, S.; Stein, R. S. *Macromolecules* **1989**, *22*, 422.
(3) Demus, D.; Richter, L. *Textures of liquid crystals*; Verlag Chemie: Weinheim, New York, 1978.
(4) Kleman, M.; Liebert, L.; Strzelecki, L. *Polymer* **1983**, *24*, 295.
(5) Rojstaczer, S.; Stein, R. S. *Mol. Cryst. Liq. Cryst.* **1988**, *157*, 293.
(6) Kerker, M. *The scattering of light and other electromagnetic radiation*; Academic Press: New York, London, 1969.
(7) Clough, S.; Van Aartsen, J. J.; Stein, R. S. *J. Appl. Phys.* **1965**, *36*, 3072.
(8) Leslie, F. M. *A.R.M.A.* **1968**, *28*, 265.
(9) Frank, F. C. *Discuss. Faraday Soc.* **1958**, *25*, 19.
(10) Dzyaloshinskij, I. E. *Sov. Phys.-JETP* **1970**, *31*, 773.
(11) Wood, B. A.; Thomas, E. L. *Nature* **1986**, *324*, 655.
(12) Hudson, S. D.; Thomas, E. L.; Lenz, R. W. *Mol. Cryst. Liq. Cryst.* **1987**, *153*, 63.
(13) Rojstaczer, S.; Hsiao, B. H.; Stein, R. S. *Polym. Prepr.* **1988**, *29*(1), 486.

Monte Carlo Simulation and Mean Field Analysis of Two-Dimensional Random Copolymer/Homopolymer Blends

J. H. van Vliet and G. ten Brinke*

Department of Polymer Chemistry, University of Groningen, Nijenborgh 16, 9747 AG Groningen, The Netherlands. *Received November 14, 1988; Revised Manuscript Received March 13, 1989*

ABSTRACT: A two-dimensional system consisting of a mixture of a random copolymer and a homopolymer is investigated in some detail. Segregation and chain interpenetration are discussed as a function of the strength of the intramolecular repulsion effect. Equations to deal with these phenomena are derived and compared with Monte Carlo simulations. The possibility that polymers which are immiscible in three dimensions become miscible in two dimensions is discussed. The Monte Carlo calculations show that, besides intermolecular chain ordering and slight chain interpenetration, the intramolecular repulsion effect induces an internal reorganization of the random copolymers. Arguments that this will be true for many blends of homopolymers as well are given.

Introduction

Some years ago,[1] Monte Carlo simulations were used to verify de Gennes's[2] prediction about polymer segregation in two-dimensional systems. A more recent paper[3] dealt with a mixture of two polymers with an attractive exchange interaction between the different segments involved. In this case interpenetration of the chains occurred. Spinodal decomposition was studied for a two-dimensional binary polymer mixture with a repulsive exchange interaction between the different segments.[4,5] A comprehensive review of Monte Carlo simulations of lattice models for macromolecules is given by Kremer and Binder.[6]

From experiments as well as mean field arguments, it is well-known that stable blends of a random copolymer and a homopolymer can exist, although mixtures of a homopolymer, comprising either kind of the monomers of the random copolymer, with the homopolymer phase separate.[7-9] This is due to the so-called intramolecular repulsion effect, a phrase which is used to indicate that the interaction between the different monomers of the random copolymer is relatively unfavorable. Closely related to this is the observation that relatively strong endothermic interactions between structural groups of the pure components are important factors in the formation of miscible homopolymer blends. One of the best known examples is the miscibility of poly(vinyl chloride) with a series of aliphatic polyesters.[10] Very recently this was also demonstrated for a large class of different polyamide blends.[11] From these and other studies, a picture of the intramolecular repulsion effect, being the real driving force for polymer–polymer miscibility in many systems, emerges.

This conclusion prompted us to investigate in some detail the behavior of a two-dimensional system consisting of a homopolymer and a random copolymer. But there are additional important advantages associated with the involvement of random copolymers. If only homopolymers are considered, the interactions are cooperative in the sense that a perfect fit between the two different polymers is possible. In real systems this is for instance observed between isotactic and syndiotactic poly(methyl methacrylate)[12] or in various polyelectrolyte mixtures, like sodium polystyrene with poly(vinylbenzyltrimethylammonium chloride).[13] Such phenomena are referred to as complexation rather than mixing.

Finally there is a third aspect, which is also not present in numerical studies on homopolymer mixtures, but which

0024-9297/89/2222-4627$01.50/0